CARBON 80 (2014) 174–182

Available at www.sciencedirect.com

ScienceDirect

journal homepage: www.elsevier.com/locate/carbon

Mussel-inspired, ultralight, multifunctional 3D nitrogen-doped graphene aerogel

Xinhong Song [a], Liping Lin [a], Mingcong Rong [a], Yiru Wang [a], Zhaoxiong Xie [c,*], Xi Chen [a,b,*]

[a] Department of Chemistry and the MOE Key Laboratory of Spectrochemical Analysis & Instrumentation, College of Chemistry and Chemical Engineering, Xiamen University, Xiamen 361005, China

[b] State Key Laboratory of Marine Environmental Science, Xiamen University, Xiamen 361005, China

[c] State Key Laboratory for Physical Chemistry of Solid Surfaces & College of Chemistry and Chemical Engineering, Xiamen University, Xiamen 361005, China

ARTICLE INFO

Article history:
Received 26 May 2014
Accepted 16 August 2014
Available online 21 August 2014

ABSTRACT

Inspired by marine mussel, an ultralight, three dimensional (3D), and nitrogen doped graphene aerogel (NGA) is developed by virtue of dopamine (DA). DA undergoes self-polymerization that can functionalize the graphene surface and also embeds nitrogen atoms onto the graphene sheets upon pyrolysis. The morphology and textural properties were investigated by scanning and transmission electron microscopy, X-ray photoelectron spectroscopy and Raman spectrum. By adjusting the amount of graphene oxide and DA in the precursor mixture, NGA with a density as low as 1.9 mg cm^{-3} can be prepared. The resultant NGA is macroscopic-assembled, mechanically stable, and fire-resistant. It has very high adsorption capacity and efficient space utilization towards oil uptake, thereby prompting practical applications as a suction skimmer in marine oil spillage or chemical leakage recovery. The high conductivity and 3D interconnected porous structure of the NGA permit good performance as electrode material for electrochemical sensors.

1. Introduction

Ultralight aerogels [1,2] have shown a thriving development in recent decades due to their excellent properties. Owing to their light-weight, porous solids with large surface areas, ultralight aerogels provide a brand new platform for many important applications such as energy storage [3], supercapacitors [4], adsorption [5], catalysis supports [6], and gas sensors [7]. Graphene, a monolayer of carbon atoms packed into a honeycomb lattice, has attracted tremendous interest in a variety of fields due to its extraordinary electron mobility, high surface area, good thermal conductivity and mechanical properties [8]. The integration of the individual graphene sheets into macroscopic structure [9] while keeping the unique properties of nanoscale building blocks is of great significance for reliable practical applications. One efficient approach to assemble graphene sheets into 3D bulk objects is to prepare them as aerogels or foams [10–15].

In addition, chemical doping is another feasible way to functionalize and tune the properties of assembled graphene

* *Corresponding authors:* Address: Department of Chemistry and the MOE Key Laboratory of Spectrochemical Analysis & Instrumentation, College of Chemistry and Chemical Engineering, Xiamen University, Xiamen 361005, China. Fax: +86 592 2184530 (X. Chen).
E-mail addresses: zxxie@xmu.edu.cn (Z. Xie), xichen@xmu.edu.cn (X. Chen).

http://dx.doi.org/10.1016/j.carbon.2014.08.054
0008-6223/

by the regulation of the carbon–carbon bonds within the planar graphene structures [16]. Incorporating heteroatoms such as nitrogen [17,18] into graphene can improve and modulate its physicochemical characteristics, especially its electrochemical performance. So far, most nitrogen doped graphene is commonly prepared using chemical vapor deposition [19], pyrolysis of a nitrogen-containing precursor such as polyaniline or polypyrrole [20], nitrogen-plasma treatments of graphene [21] and thermal annealing with ammonia [22] or pyrrole [23]. These methods can successfully anchor nitrogen atoms onto the graphene nanosheets, increasing their electrocatalytic activity by providing more active sites. However, many of these approaches require toxic gas precursors, or a large well-ordered template. Therefore, it is desirable to develop a template-free and low-cost strategy starting from nontoxic nitrogen resources to obtain multifunctional, macroscopic nitrogen doped graphene architecture.

Marine mussels [24] are the true masters of adhesion. At a molecular level, the adhesive proteins [25] of mussels are heavily decorated with Dopa (3,4-dihydroxy-L-phenylalanine), a catecholic functionality. Dopamine (DA), containing catechol and amine groups, is a unique molecule mimicking the adhesive proteins; it can spontaneously polymerize into polydopamine (PDA) to modify virtually all types of material surfaces, regardless of their chemical functionality or surface energy, therefore, its polymeric form can be used as a good adhesive [26,27]. Herein, a novel design of 3D nitrogen (N) doped graphene aerogel (GA) is developed by incorporating mussel-inspired chemical motif of dopamine. DA performs oxidative polymerization that can reduce and functionalize the surface of graphene, while graphene sheets are assembled into 3D porous structures. DA also serves as a source of nitrogen by introducing N atoms onto the graphene nanosheets upon pyrolysis. In contrast with other N containing precursors, DA is a widespread and sustained natural resource.

2. Experimental

2.1. Preparation of ultralight 3D NGA

Graphene oxide (GO) sheets were synthesized from graphite powder (Sigma–Aldrich) based on the well-known Hummers' method but with some modification [28,29]. The NGA hydrogel was prepared using the following procedure. Typically, DA (15 mg) was added into a GO aqueous dispersion (15 mL, 1 mg mL^{-1}) with pH adjusted to about 8.0, and sonicated for 40 min. The color of the solution gradually changed to pale brown. The mixture was then sealed in a 20 mL Teflon-lined autoclave and maintained at 180 °C for 12 h to form an N-containing gel. After the autoclave was naturally cooled down to room temperature, the as-prepared hydrogel was taken out and washed using ethanol and water and then freeze-dried. Ultralight NGA was obtained after heating the freeze-dried graphene gel at 800 °C for 3 h under an Ar atmosphere. NGA (with a range of volumes and densities) was prepared under the same conditions except for using different concentrations of GO (0.2–4.0 mg mL^{-1}) and the ratio of GO to DA by weight was kept consistent at 1:1.

2.2. Preparation of 3D GA

3D GA was synthesized based on the hydrothermal method [9]. Typically, a 15 mL portion of 1 mg mL^{-1} homogeneous GO aqueous dispersion was sealed in a 20 mL Teflon-lined autoclave and maintained at 180 °C for 12 h. Then the autoclave was naturally cooled to room temperature and the as-prepared hydrogel was taken out, washed with ethanol and water. The hydrogel was then freeze-dried and annealed at 800 °C for 3 h under an Ar atmosphere.

2.3. Preparation of pristine graphene

The as-prepared GO sheets were chemically reduced using hydrazine vapor at 90 °C for 24 h, followed by vacuum-drying at 160 °C for 24 h.

2.4. Characterization

2.4.1. Density measurement and determination of the NGA monoliths

The densities (ρ) of the monoliths could be obtained by the following two methods:

(a) The density of NGA could be determined from the mass weight divided by the volume. Here, the averaged values of data were used.

The volumes (v) of cylindrical shaped aerogel monolith was calculated based on Eq. (E1)

$$v = \pi(2/d)^2 h \quad \text{(E1)}$$

d refers to the diameter of NGA monoliths, and h represents the height of NGA monoliths. The densities ρ of NGA were calculated from Eq. (E2)

$$\rho = m/v \quad \text{(E2)}$$

m refers to the mass of the NGA obtained by the precision balance (METTLER TOLEDO XS205).

(b) Densities were determined by a balance (METTLER TOLEDO XS205) equipped with accessories for the density determination by the Archimedes principle. The results for NGA obtained from the two methods are almost in agreement.

The morphology of the as prepared samples was investigated using scanning (SEM, Hitachi S4800 and LEO 1530 field-emission system) and transmission electron microscopy (TEM). The morphology of the NGA was observed using TEM and HRTEM on a JEM-2100 transmission electron microscope with an acceleration voltage of 200 kV. All TEM samples were prepared by depositing a drop of diluted suspension in ethanol on a copper grid coated with carbon film.

The specific surface areas and pore size distributions of the materials were calculated using the Brunauer–Emmett–Teller (BET) and Barrett–Joyner–Halenda (BJH) methods, respectively. Nitrogen adsorption experiments were conducted at 77.4 K using TriStarII3020 (Micromeritics Instrument Corporation) apparatus. Before adsorption measurements, the samples were degassed in vacuum at 473 K for 3 h.

Electronic binding energies were measured using X-ray photoelectron spectroscopy (XPS) analysis which was performed on a PHI Quantum 2000 Scanning ESCA Microprobe with a monochromatized microfocused Al X-ray source. All the binding energies were calibrated using the C1s as reference energy (C1s = 284.6 eV). Elemental composition was determined with Elementar Vario EL III.

Thermogravimetric analysis (TGA) measurements were carried out using a simultaneous thermal analyzer STA-449 under a nitrogen atmosphere increasing from room temperature to 1000 °C at 10 °C min^{-1}.

The Raman spectrum was investigated using nanophoton Raman 11 with excitation wavelength: 532.00 nm; laser current: 100%; excitation power: 3.243309 mW. The intensity ratio of the D and G bands (I_D/I_G) is inversely proportional to the in-plane crystallite sizes L_a [30,31]. The crystallite size can be determined based on the Tuinstra–Koenig relationship [32,33], Eq. (E3):

$$L_a\,(\mathrm{nm}) = (2.4 \times 10^{-10})\lambda^4 (I_D/I_G)^{-1} \quad \text{(E3)}$$

λ is the Raman excitation wavelength (λ = 532 nm).

X-ray powder diffraction (XRD) results were collected with a Panalytical X'pert PRO (PANalytical B.V., Netherlands) equipped with graphite monochromatized high-intensity Cu-Ka radiation (λ = 1.5417 Å).

Electrical conductivity was measured using the four-probe method with metal electrodes attached to the ends of cylindrical samples. The amount of current transmitted through the sample during measurement was 100 mA, and the voltage drop along the sample was measured over distances of about 5 mm. Six or more measurements were taken on each sample, and results were averaged. Bulk densities of the samples were determined from the physical dimensions and mass of each sample.

The dynamic rheological measurements of the NGA and GA were performed by a Rheometer Anton Paar Physica MCR301 with parallel-plate geometry (CP25-2) at 25 °C. Dynamic frequency sweep experiments were measured from 1 to 100 rad/s with the distance of two plates fixed at 1 mm and the oscillatory strain at 0.2%. Temperature sweep experiments from 25 to 100 °C were investigated at a heating rate of 5 °C/min.

2.5. *Electrochemical measurements*

Cyclic voltammetry (CV) and differential pulse voltammogram (DPV) behavior of NGA modified electrodes were investigated on a CHI660B electrochemical workstation in three-electrode systems. A conventional three-electrode system included a glassy carbon electrode (GCE) coated with catalyst film, a silver auxiliary electrode and a saturated calomel reference electrode (SCE). All potentials reported in this paper refer to the SCE scale.

In the three-electrode system, the GCE was polished successively using 0.3 and 0.5 mm Al_2O_3 powder and rinsed thoroughly with ethanol and water each for 5 min, and then dried in blowing N_2. 5 mg GA and 5 mg NGA were dispersed in N,N-Dimethylformamide using ultrasonication for 30–40 min, and resulted in a 1 mg mL^{-1} suspension. 7 μL GA and NGA suspension were then pipetted onto the prepared GCE surface separately and dried at room temperature.

3. Results and discussion

The synthetic procedure of NGA production is depicted in Fig. 1 with two steps: (1) in-situ hydrothermal cross-linking and polymerization of the mixture at 180 °C for 12 h to obtain the 3D hybrid N-containing precursor. The resultant hydrogel exhibited negligible volume dilation after the hydrothermal treatment (Fig. S1). During this process, the DA turned to intermediate dihydroxyindole by liberating protons, and formed PDA between individual GO sheets. Instead of the weak van der Waals interaction and the hydrogen bonding force between GO sheets and water, the intercalating PDA effectively formed a strong adhesive force with the GO sheets. Reduction of the GO sheets simultaneously occurred by the oxidative polymerization of DA and, thus, DA guided the graphene sheets to blossom into a 3D structure. (2) An annealing step at 800 °C under an Ar atmosphere for 3 h was carried out to convert the N source obtained from the first step to an N doped character. It is important to know that DA played multi-functional roles in this method: as a catecholic anchor, it chemisorbed to the surfaces of GO to form an adherent PDA coating, which then acted as a covalent

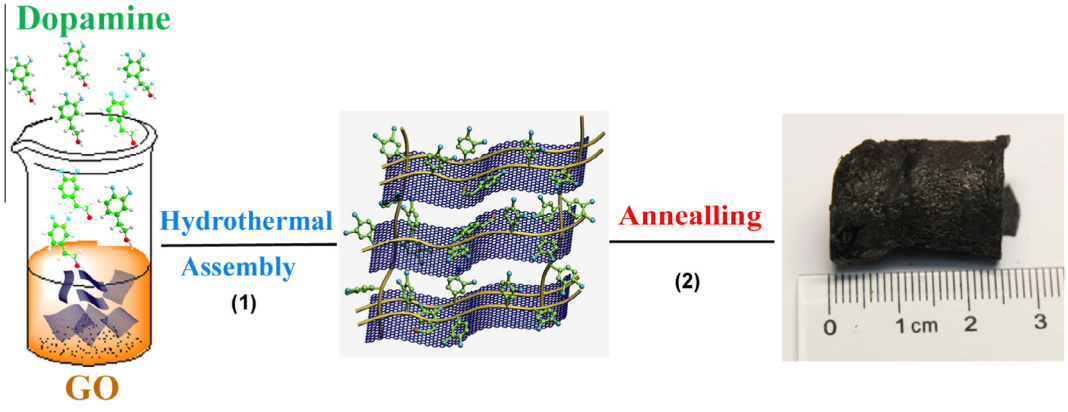

Fig. 1 – Illustration of the production process of the ultralight 3D NGA. (A colour version of this figure can be viewed online.)

cross-linking unit: as a reducing agent, the partial overlapping or coalescence of the GO sheets was readily reduced by DA with simultaneous capping by PDA to prevent the reduced GO sheets from agglomeration or restacking; and, as the direct N source, after the functionalization of the graphene surface, DA then introduced nitrogen atoms onto the graphene sheets upon pyrolysis.

The resulting NGA was macroscopic-assembled and ultralight. As shown in Fig. 2a, two NGAs can stand stably on the top of the red *Calliandra haematocephala* flower without deforming it at all (more digital photos of NGA are shown in Fig. S2). Varying with the concentration of the precursors, NGA provided ultra-low densities ranging from 1.9 to 6.0 mg cm^{-3}. The lowest density was comparable to the lightest silica aerogels (1 mg cm^{-3}) [2] and the N doped graphene framework (2.1 ± 0.3 mg cm^{-3}) [22]. When mixed with the same weight of DA, a low concentration (0.2 mg mL^{-1}) of homogeneous GO aqueous permitted the assembly of 3D network architecture, and this phenomenon did not occur in the absence of DA. By increasing the concentration of the mixture (the weight ratio of GO to DA was kept at 1:1) or scaling up the autoclave, we can obtain larger volume of NGA (Fig. S3). The as-prepared products showed black cork-like morphology. As revealed in the SEM image (Fig. 2b), the twisted nanosheets were randomly cross-linked to form a network structure with rich nano and micropores interpenetrating inside. The skeleton of the NGA was dissected and investigated using TEM. As shown in Fig. 2c, the corrugated nanoflakes of the NGA exhibited a typical wrinkled and crumbled structure, and the HRTEM (Fig. 2d) confirmed that the thin walls typically consisted only of a few layers of graphene sheets. X-ray powder diffraction (Fig. S4) further proved the production of high-quality graphene sheets.

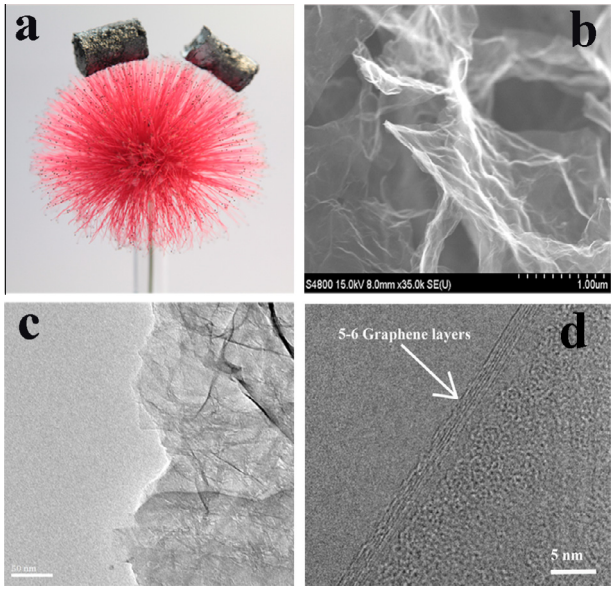

Fig. 2 – (a) Photograph of two NGAs (cylinder size: diameter 1.9 cm, length 1.2 cm) standing on a *Calliandra haematocephala* flower. (b) SEM image of the sample in (a). (c) Typical TEM image of the NGA. (d) HRTEM image of the NGA. (A colour version of this figure can be viewed online.)

The specific surface area and pore size distribution of the NGA were calculated using the BET and BJH methods. The NGA possessed a specific high surface area approximating 322.6 m^2 g^{-1} (Fig. S5), which was higher than that of the 3D nitrogen and boron co-doped graphene [34].

The composition of the NGA was examined using XPS measurement. In the XPS spectrum of the NGA (Fig. 3a), the peaks appeared at about 401, 284.8 and 532.7 eV corresponding to N1s, C1s and O1s, with the N/C atomic ratio of 3.5%, which proved doping of the N atoms. Moreover, as shown in the high-resolution N1s XPS spectra (Fig. 3b), the N atoms were in three different valence states (pyridinic-N, graphitic-N and quaternary-N) in the graphene skeleton, suggesting that the N atoms were incorporated into the carbon–carbon bonds of the graphene. The electroactive pyridinic-N and graphitic-N played a dominant role in the NGA. Pyridinic-N (398.5 eV) could improve the onset potential and the electrochemical performance more obviously than those of other N species in the carbon materials; the appearance of pyrrolic-N (399.3 eV) was ascribed to the contribution of pyridone and pyrrol; the quaternary-N (400.8 eV) was derived from the N atoms that replace the C atoms in the graphene hexagonal-ring, suggesting that the N atoms were incorporated into the carbon–carbon bonds of the graphene. The schematic illustration of the chemical structure of NGA is shown in Fig. 3c. The C1s peak can be deconvoluted into three peaks owing to the doping of nitrogen atoms into graphene (Fig. S6). Raman spectroscopy is another way to evaluate the doping effect of graphene. The D band arises because of the structural disorder or defects present in graphitic based materials; whereas the G band arises from sp^2 bonded ordered graphitic carbon [33]. As shown in Fig. 3d, the small D peak of pristine graphene (PG) indicated the absence of significant defects. As for the 3D GA, the large amounts of hydroxyl and epoxy groups originating from the hydrothermal step reduced the relative amount of sixfold aromatic rings, thus increasing the intensity of the D band while decreasing the G band. When nitrogen atoms were doped into the graphene sheets, the substitution of nitrogen atoms was usually accompanied by the introduction of defects such as bonding disorders and vacancies in the graphene lattice, and therefore these defects would raise the D band of NGA even higher. Furthermore, compared with PG, the G band of NGA exhibited a blue shift of 6 cm^{-1}, which was similar to N-doped graphene synthesized using the arc discharge method [35]. The ratio of D to G band intensity (I_D/I_G) [33] is commonly utilized to gauge the degree of structural disorder, with higher values suggesting more disorder along with smaller average graphitic crystalline size (L_a). The I_D/I_G values of the PG, GA and NGA were 0.26, 1.06 and 1.21, which corresponded to the calculation of the crystallite size of 74, 18 and 16 nm [Eq. (E3)]. As a consequence, together with the nitrogen doping, the crystallite size of the NGA decreased as anticipated. We also investigated whether the intensity ratio of I_D/I_G changed when the initial concentration of DA varied (Fig. 3f). The increasing initial concentration of DA led to increasing N doped atoms, which caused a concomitant increase of the intensity ratio of I_D/I_G.

Although the NGA had an ultralight weight, its load bearing ability was remarkable. As shown in Fig. 4a, 10 mg of NGA was able to support 5000 fold its own weight without

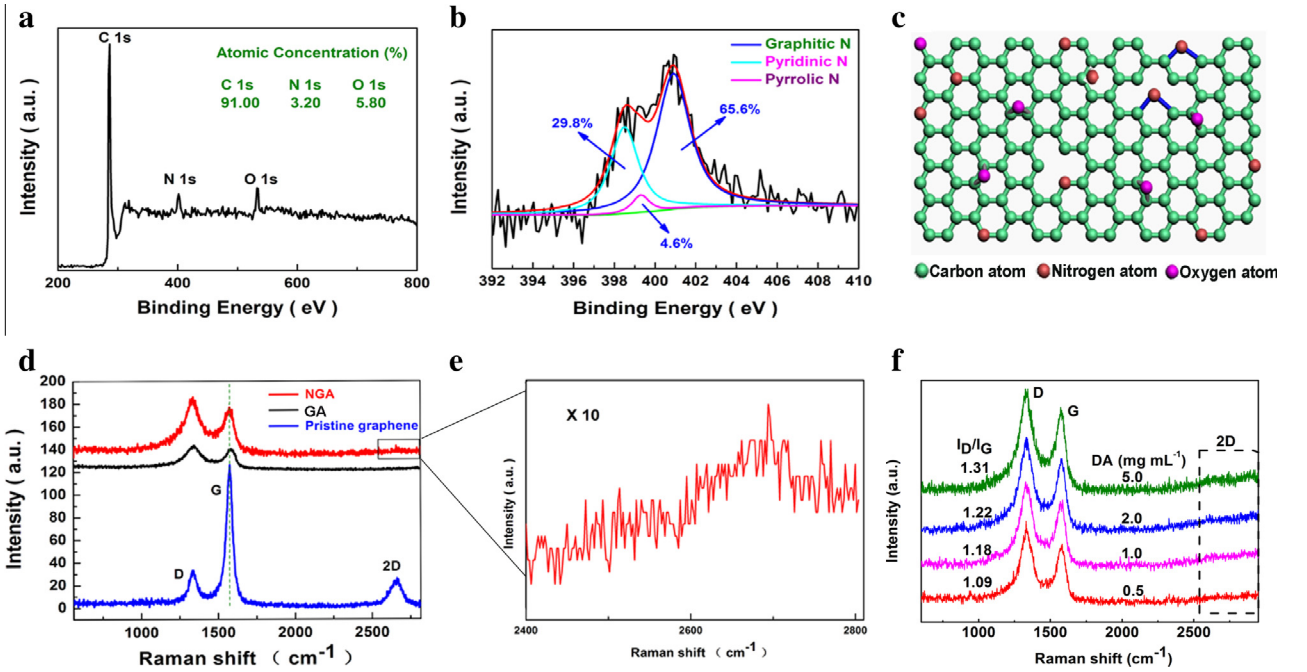

Fig. 3 – (a) XPS spectrum of the NGA and (b) the corresponding high-resolution N1s peak. (c) Schematic illustration of the chemical structure of the NGA. (d) Raman spectra of pristine graphene, GA and the NGA, where D, G and 2D denote the characteristic D band, G band and 2D band of graphene. (e) Magnified spectra of the dashed box of the 2D band (the excitation wavelength is 532 nm). (f) Raman spectra of the NGA with different initial concentrations of DA. (A colour version of this figure can be viewed online.)

collapsing. The NGA was also fire-resistant. Fig. 4b and c described that the inherent 3D porous structure survived and remained intact after burning repeatedly under an ambient atmosphere (Movie S1). Since the strong adhesion force formed between DA and graphene sheets, which was up to covalent bonding force [24,25], NGA had a reinforced mechanical behavior than that of GA. The rheological measurements as shown in Fig. S7 further revealed that the mechanical property and thermal stability of NGA were much more superior to that of the undoped GA. In addition, the NGA was electrically conductive (Fig. 4d) with a high conductivity of 2.62×10^2 S m^{-1}, and its ultralight weight led to pronounced electrostatic effects (Movie S2). The density, textural properties, and bulk conductivity of GA and NGA are summarized in Table S1.

Because of its surface hydrophobicity (Fig. 4e and f), high porosity and mechanically stable graphene skeleton, the NGA is an ideal candidate for highly efficient separation/extraction of specific substances, such as organic pollutants and oils. As shown in Fig. 5a, the NGA can absorb gasoline (dyed with Sudan III) within seconds while repelling the water (Movie S3), thereby prompting practical applications as a suction skimmer in marine oil spillage or chemical leakage recovery. The NGA showed excellent adsorption capacity (Fig. 5b and c) for various classes of organic liquids, e.g., commercial petroleum products, vegetable oil and different carbon chain lengths of chemical agent. The efficiency of oil adsorption can be referred to as weight ratio, i.e., the ratio of the final weight after full adsorption to the initial weight of NGA (Fig. 5b).

In particular, NGA showed the capacity to uptake amounts of liquids up to 40 to 156 times of their own weight, which was higher than 3D GAs (13–37 times) [11,36], spongy graphene (20–86 times) [5], carbon nanofiber aerogels (40–115 times) [37], hybrid graphene/carbon nanotube foams (80–130 times) [38], and close to carbon nanotube sponges (80–180 times) [39], but lower than N-doped graphene framework (200–600 times) [23] and ultra-flyweight aerogel (215–714 times) [12]. Since the mass-based adsorption capacity is strongly affected by the density of oils and absorbing materials, therefore we also used volume-based adsorption capacity (V_{oil}/V_{NGA}) to test the adsorption ability of NGA (Fig. 5c). The volume adsorption capacities of the NGA for oils or other organic liquids were higher than 74%, indicating that most of the porous volume was used for oil storage.

The above results demonstrated that the NGA was of comparable oil storage ability to the previously reported carbonaceous materials such as carbon nanotube sponges (70–140% for hexane and 60–120% for chloroform) [36] and N-doped graphene framework (78.1% for gasoline) [23], but higher than ultra-flyweight aerogel (26% for petrol oil) [12]. Therefore, although the NGA showed lower mass gain capacity than some of the carbonaceous aerogels, it still exhibited one of the most efficient space utilizations towards oil uptake. The reason for this high adsorption capacity was that oils were stored mainly in the interconnected pores formed by the oleophilic walls of the doped graphene sheets. The absorbed oil or solvents can be removed by direct combustion in air for recycled use of the NGA (Fig. S8).

Different from other 2D materials, NGA can provide a unique 3D interconnected porous structure with access to the N active sites within exposed graphene sheets and

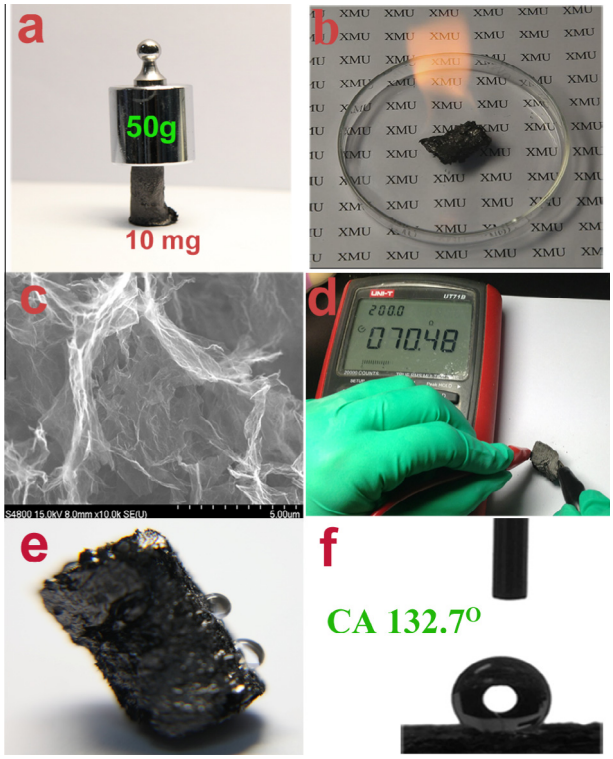

Fig. 4 – (a) Photographs of a 10 mg NGA supporting a 50 g weight and (b) a burning NGA. (c) SEM image of the burned NGA. (d) Electrical conductivity of NGA. (e) Water droplets leaning on the surface of an NGA sample proving the hydrophobicity of NGA. (f) Water contact measure of NGA, the contact angle is 132.7°. (A colour version of this figure can be viewed online.)

multidimensional electron transport pathways, thus NGA is regarded as a promising electrode material for chemical sensors. Biomolecules such as ascorbic acid (AA), DA and uric acid (UA) play important roles in physiological bodily functioning of organisms. They coexist in body fluids but their differences or maladjustment of their concentration levels may induce cancer, Parkinson's disease, Huntington's diseases, schizophrenia, etc. [40–42]. Therefore, the determination of AA, DA and UA is of great importance for both developing nerve physiology and diagnosis combined with medicine control. The concentrations of AA and UA are generally much higher than that of DA (100–1000 folds) in biological fluids, and this offers greater ability to determine one of the three. Many methods have been developed for the determination of these biological substances, but the electroanalytical method [43–45] is proved to be a very promising strategy. However, electrochemical determination of these species based on anodic oxidation suffers from the oxidation peaks severely overlapping with solid electrodes [46]. Since NGA thrives as an electroactive material, herein, we used 3D NGA to build an electrochemical sensor to accomplish simultaneous determination of UA, DA and AA.

The CV behaviors of AA, DA and UA were investigated using a bare GCE, a GA modified GCE (GA/GCE) and a NGA modified GCE (NGA/GCE). As shown in Fig. 6a, in PBS (pH 7.4), AA was negatively charged, and the oxidation peak of AA corresponded to the oxidation of hydroxyl groups to carbonyl groups. The formation of hydrogen bonds between the NGA microlayers and AA may increase the electron transfer. For DA, a well-defined redox couple with a peak separation of 64 mV on the NGA/GCE showed much better reversibility than using the bare GCE (ΔE = 399 mV) (Fig. S9a) and GA/GCE (ΔE = 259 mV) (Fig. S9b). This improved reversibility could be

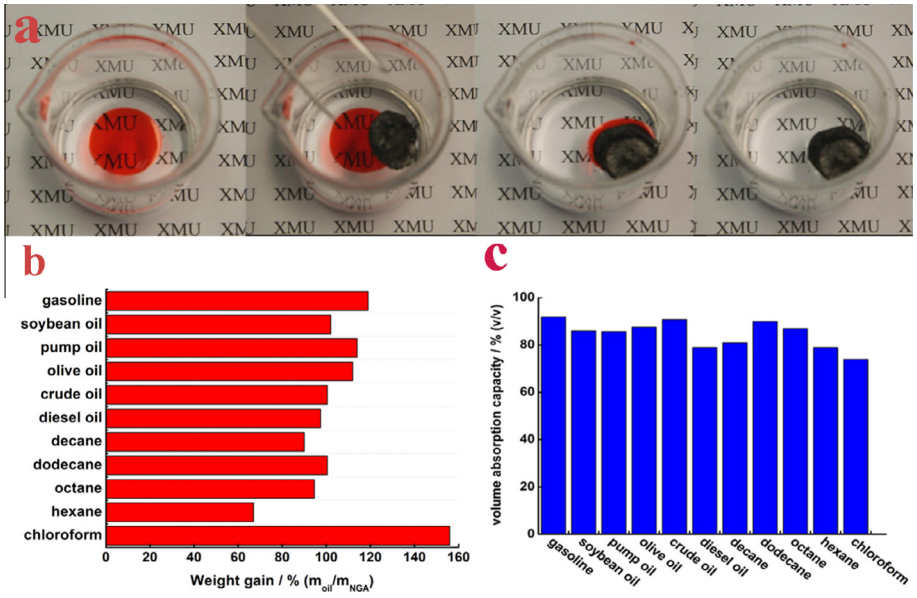

Fig. 5 – (a) NGA adsorbing gasoline dyed with Sudan III (see Movie S2). (b) Weight-based and (c) volume-based adsorption capacities of the NGA (with a density of 5.0 mg cm^{-3}) for oils and organic solvents. (A colour version of this figure can be viewed online.)

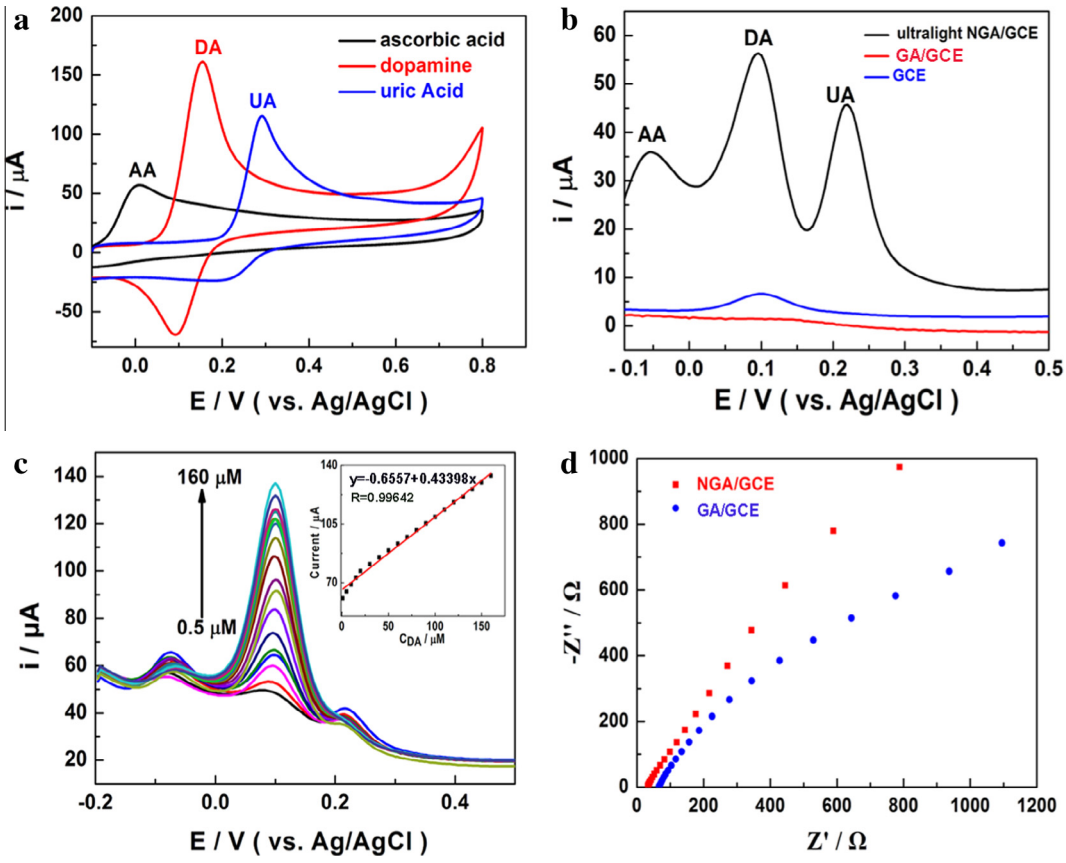

Fig. 6 – (a) Cyclic voltammograms of 1.0 mM AA, 1.0 mM DA and 1.0 mM UA in 0.10 M PBS (pH 7.4) at NGA/GCE with a scan rate of 100 mV/s. (b) Differential pulse voltammogram (DPV) for 1.0 mM AA, 0.050 mM DA and 0.10 mM UA in 0.10 M PBS (pH 7.4) at NGA/GCE, GA/GCE and GCE. (c) DPV for different concentrations of DA from 0.50to 160 μM containing 1.0 mM AA and 50 μM UA at NGA/GCE. Inset: plots of the anodic peak current as a function of DA concentrations. (d) Electrochemical impedance spectroscopy of NGA/GCE and GA/GCE in 2.5 mM $[Fe(CN)_6]^{3-}/[Fe(CN)_6]^{4-}$ containing 0.10 M KCl. The frequency range was selected from 0.01 to 10^5 Hz with a perturbation amplitude of 5 mV. The initial potential was 0.10 V. (A colour version of this figure can be viewed online.)

traced back to the interaction between the graphene layers of the NGA and the benzene ring of the DA molecule. Moreover, the hydrogen bonds between the doped nitrogen atoms within the NGA layers and the hydroxyl or amine groups from DA molecule enhanced the electron transfer kinetics. UA showed quasi-reversible electrochemical behavior with oxidation/reduction peaks on the NGA/GCE, revealing that UA was first oxidized to quinonoid, and then experienced a rapid chemical reaction, which matched to an EC mechanism [47]. Compared to the bare GCE and GA/GCE, the oxidation potential of AA, DA and UA was distinctly negative shifted and well separated, in addition to the much higher oxidation currents using the NGA/GCE. The difference of their oxidation potentials was large enough to distinguish each other, indicating that NGA accelerated the oxidation of AA, DA and UA, and thus decreased their overpotentials, which is the key factor to realize their simultaneous determination. DPV is a sensitive way to undertake electrochemical detection [48]. In a mixture of 1.0 (AA), 0.05 (DA) and 0.10 mM (UA) in 0.10 M PBS (pH 7.4), the oxidation peaks of AA and DA completely overlapped and showed a broad overlapping peak at about 160 and 110 mV on the GCE and GA/GCE. On the contrary, three well shaped oxidation peaks (Fig. 6b) were resolved using NGA/GCE with larger peak potential difference and current intensity. The peak potentials were at about −52, 96 and 220 mV for AA, DA and UA and with separations of 148, 134 and 272 mV for AA–DA, DA–UA and AA–UA. The fast heterogeneous electron kinetics of these molecules on the NGA and the enlarged separations coupled with the higher sensitivity confirmed that NGA could facilitate the determination of AA, DA and UA simultaneously. Furthermore, we also used the NGA/GCE to investigate the individual determination of DA in the ternary mixture, and the experiment results revealed that the oxidation current linearly increased with the addition of DA from 0.50 to 160 μM in the presence of 1.0 mM AA and 50 μM UA. It was found that the addition of DA into the electrochemical cell did not have significant influence on the peak currents or peak potentials of the other two biomolecules (Fig. 6c). It clearly showed that the analytical parameters of DA including detection limit (0.20 μM) and linear range using NGA/GCE were better or comparable to the previous reports on using different kinds of modified electrodes [49]. An equivalent 5.0 mM $[Fe(CN)_6]^{3-/4-}$ redox couple was used to explore the interface properties of the NGA modified

electrodes. As expected (Fig. 6d), the NGA/GCE showed an almost straight tail line and better ability to promote the electron transfer than that of the GA/GCE due to the nitrogen doping and the particular 3D microstructure with multiple electron paths. The above results proved that NGA possessed preferable electroactivity in neutral media and displayed excellent electrocatalytic activity towards the oxidation of AA, DA and UA.

4. Conclusions

We developed a novel strategy for the preparation of an ultralight, multifunctional 3D NGA. Benefiting from the self-polymerization and adhesion of DA, the embedding of DA in GO aqueous would change the product morphology dramatically and offer an N doped 3D porous structure. The resulting NGA presented an ultralow density of 1.9 mg cm^{-3}, high adsorption capacity and efficient space utilizations towards organic pollutants or oils. Based on the 3D open-pore structure and nitrogen doping, the NGA exhibited excellent electrochemical activity towards the oxidation of AA, DA and UA in neutral media. With a clever choice and combination of natural phenomena, more and more versatile macroscopic-assembled graphene-based architecture will become available for wider applications.

Acknowledgments

This research work was financially supported by the National Basic Research Program of China (2010CB732402), the National Nature Scientific Foundation of China (Nos. 1175112 and 21375112) and NFFTBS (No. J1030415), which are gratefully acknowledged. We thank Professor John Hodgkiss of The University of Hong Kong for assistance with English in the paper.

Appendix A. Supplementary data

Supplementary data associated with this article can be found, in the online version, at http://dx.doi.org/10.1016/j.carbon.2014.08.054.

REFERENCES

[1] Hüsing N, Schubert U. Aerogels—airy materials: chemistry, structure, and properties. Angew Chem 1998;37(1–2):22–45.
[2] Hotaling SP. Ultra-low density aerogel optical applications. J Mater Res 1993;8(02):352–5.
[3] Su Y, Zhang Y, Zhuang X, Li S, Wu D, Zhang F, et al. Low-temperature synthesis of nitrogen/sulfur co-doped three-dimensional graphene frameworks as efficient metal-free electrocatalyst for oxygen reduction reaction. Carbon 2013;62:296–301.
[4] Dong X-C, Xu H, Wang X-W, Huang Y-X, Chan-Park MB, Zhang H, et al. 3D graphene–cobalt oxide electrode for high-performance supercapacitor and enzymeless glucose detection. ACS Nano 2012;6(4):3206–13.
[5] Bi H, Xie X, Yin K, Zhou Y, Wan S, He L, et al. Spongy graphene as a highly efficient and recyclable sorbent for oils and organic solvents. Adv Funct Mater 2012;22(21):4421–5.
[6] Wu Z-S, Yang S, Sun Y, Parvez K, Feng X, Müllen K. 3D nitrogen-doped graphene aerogel-supported Fe_3O_4 nanoparticles as efficient electrocatalysts for the oxygen reduction reaction. J Am Chem Soc 2012;134(22):9082–5.
[7] Yavari F, Chen Z, Thomas AV, Ren W, Cheng H-M, Koratkar N. High sensitivity gas detection using a macroscopic three-dimensional graphene foam network. Sci Rep 2011:1.
[8] Geim AK, Novoselov KS. The rise of graphene. Nat Mater 2007;6(3):183–91.
[9] Xu Y, Sheng K, Li C, Shi G. Self-assembled graphene hydrogel via a one-step hydrothermal process. ACS Nano 2010;4(7):4324–30.
[10] Chen Z, Ren W, Gao L, Liu B, Pei S, Cheng H-M. Three-dimensional flexible and conductive interconnected graphene networks grown by chemical vapour deposition. Nat Mater 2011;10(6):424–8.
[11] Cong H-P, Ren X-C, Wang P, Yu S-H. Macroscopic multifunctional graphene-based hydrogels and aerogels by a metal ion induced self-assembly process. ACS Nano 2012;6(3):2693–703.
[12] Hu H, Zhao Z, Wan W, Gogotsi Y, Qiu J. Ultralight and highly compressible graphene aerogels. Adv Mater 2013;25(15):2219–23.
[13] Qian Y, Ismail IM, Stein A. Ultralight, high-surface-area, multifunctional graphene-based aerogels from self-assembly of graphene oxide and resol. Carbon 2014;68:221–31.
[14] Sun H, Xu Z, Gao C. Multifunctional, ultra-flyweight, synergistically assembled carbon aerogels. Adv Mater 2013;25(18):2554–60.
[15] Wu ZY, Li C, Liang HW, Chen JF, Yu SH. Ultralight, flexible, and fire-resistant carbon nanofiber aerogels from bacterial cellulose. Angew Chem 2013;52(10):2925–9.
[16] Wang H, Maiyalagan T, Wang X. Review on recent progress in nitrogen-doped graphene: synthesis, characterization, and its potential applications. ACS Catal 2012;2(5):781–94.
[17] Qu L, Liu Y, Baek J-B, Dai L. Nitrogen-doped graphene as efficient metal-free electrocatalyst for oxygen reduction in fuel cells. ACS Nano 2010;4(3):1321–6.
[18] Wang Y, Shao Y, Matson DW, Li J, Lin Y. Nitrogen-doped graphene and its application in electrochemical biosensing. ACS Nano 2010;4(4):1790–8.
[19] Gao H, Song L, Guo W, Huang L, Yang D, Wang F, et al. A simple method to synthesize continuous large area nitrogen-doped graphene. Carbon 2012;50(12):4476–82.
[20] Nguyen DD, Tai NH, Lee SB, Kuo WS. Superhydrophobic and superoleophilic properties of graphene-based sponges fabricated using a facile dip coating method. Energy Environ Sci 2012;5(7):7908–12.
[21] Jeong HM, Lee JW, Shin WH, Choi YJ, Shin HJ, Kang JK, et al. Nitrogen-doped graphene for high-performance ultracapacitors and the importance of nitrogen-doped sites at basal planes. Nano Lett 2011;11(6):2472–7.
[22] Li X, Wang H, Robinson JT, Sanchez H, Diankov G, Dai H. Simultaneous nitrogen doping and reduction of graphene oxide. J Am Chem Soc 2009;131(43):15939–44.
[23] Zhao Y, Hu C, Hu Y, Cheng H, Shi G, Qu L. A versatile, ultralight, nitrogen-doped graphene framework. Angew Chem 2012;51(45):11371–5.
[24] Lee H, Dellatore SM, Miller WM, Messersmith PB. Mussel-inspired surface chemistry for multifunctional coatings. Science 2007;318(5849):426–30.
[25] Lee BP, Messersmith PB, Israelachvili JN, Waite JH. Mussel-inspired adhesives and coatings. Annu Rev Mater Res 2011;41(1):99–132.

[26] Lee H, Rho J, Messersmith PB. Facile conjugation of biomolecules onto surfaces via mussel adhesive protein inspired coatings. Adv Mater 2009;21(4):431–4.
[27] Ryu J, Ku SH, Lee H, Park CB. Mussel-inspired polydopamine coating as a universal route to hydroxyapatite crystallization. Adv Funct Mater 2010;20(13):2132–9.
[28] Hummers WS, Offeman RE. Preparation of graphitic oxide. J Am Chem Soc 1958;80(6):1339.
[29] Becerril HA, Mao J, Liu Z, Stoltenberg RM, Bao Z, Chen Y. Evaluation of solution-processed reduced graphene oxide films as transparent conductors. ACS Nano 2008;2(3):463–70.
[30] Tuinstra F, Koenig JL. Raman spectrum of graphite. J. Chem. Phys 1970;53(3):1126–30.
[31] Ferrari A, Meyer J, Scardaci V, Casiraghi C, Lazzeri M, Mauri F, et al. Raman spectrum of graphene and graphene layers. Phys Rev Lett 2006;97(18):187401.
[32] Das A, Pisana S, Chakraborty B, Piscanec S, Saha SK, Waghmare UV, et al. Monitoring dopants by Raman scattering in an electrochemically top-gated graphene transistor. Nat Nano 2008;3(4):210–5.
[33] Cancado L, Takai K, Enoki T, Endo M, Kim Y, Mizusaki H, et al. General equation for the determination of the crystallite size L_a of nanographite by Raman spectroscopy. Appl Phys Lett 2006;88(16). 163106–3.
[34] Wu Z-S, Winter A, Chen L, Sun Y, Turchanin A, Feng X, et al. Three-dimensional nitrogen and boron co-doped graphene for high-performance all-solid-state supercapacitors. Adv Mater 2012;24(37):5130–5.
[35] Panchakarla LS, Subrahmanyam KS, Saha SK, Govindaraj A, Krishnamurthy HR, Waghmare UV, et al. Synthesis, structure, and properties of boron- and nitrogen-doped graphene. Adv Mater 2009;21(46):4726–30.
[36] Niu Z, Chen J, Hng HH, Ma J, Chen X. A leavening strategy to prepare reduced graphene oxide foams. Adv Mater 2012;24(30):4144–50.
[37] Liang H-W, Guan Q-F, Chen L-F, Zhu Z, Zhang W-J, Yu S-H. Macroscopic-scale template synthesis of robust carbonaceous nanofiber hydrogels and aerogels and their applications. Angew Chem 2012;51(21):5101–5.
[38] Worsley MA, Kucheyev SO, Mason HE, Merrill MD, Mayer BP, Lewicki J, et al. Mechanically robust 3D graphene macroassembly with high surface area. Chem Commun 2012;48(67):8428–30.
[39] Gui X, Wei J, Wang K, Cao A, Zhu H, Jia Y, et al. Carbon nanotube sponges. Adv Mater 2010;22(5):617–21.
[40] Anderson RF, Harris TA. Dopamine and uric acid act as antioxidants in the repair of DNA radicals: implications in Parkinson's disease. Free Radic Res 2003;37(10): 1131–6.
[41] Arrigoni O, De Tullio MC. Ascorbic acid: much more than just an antioxidant. Biochim Biophys Acta Gen Subj 2002; 1569(1–3):1–9.
[42] Wightman RM, May LJ, Michael AC. Detection of dopamine dynamics in the brain. Anal Chem 1988;60(13):769A–79A.
[43] Wang Z, Liu J, Liang Q, Wang Y, Luo G. Carbon nanotube-modified electrodes for the simultaneous determination of dopamine and ascorbic acid. Analyst 2002;127(5):653–8.
[44] Zare HR, Rajabzadeh N, Nasirizadeh N, Mazloum Ardakani M. Voltammetric studies of an oracet blue modified glassy carbon electrode and its application for the simultaneous determination of dopamine, ascorbic acid and uric acid. J Electroanal Chem 2006;589(1):60–9.
[45] Han D, Han T, Shan C, Ivaska A, Niu L. Simultaneous determination of ascorbic acid, dopamine and uric acid with chitosan-graphene modified electrode. Electroanalalysis 2010;22(17–18):2001–8.
[46] Zhu S, Li H, Niu W, Xu G. Simultaneous electrochemical determination of uric acid, dopamine, and ascorbic acid at single-walled carbon nanohorn modified glassy carbon electrode. Biosens Bioelectron 2009;25(4):940–3.
[47] Safavi A, Maleki N, Moradlou O, Tajabadi F. Simultaneous determination of dopamine, ascorbic acid, and uric acid using carbon ionic liquid electrode. Anal Biochem 2006;359(2):224–9.
[48] Bao Y, Song J, Mao Y, Han D, Yang F, Niu L, et al. Graphene oxide-templated polyaniline microsheets toward simultaneous electrochemical determination of AA/DA/UA. Electroanalysis 2011;23(4):878–84.
[49] Yang X, Feng B, He X, Li F, Ding Y, Fei J. Carbon nanomaterial based electrochemical sensors for biogenic amines. Microchim Acta 2013;180(11–12):935–56.